Journal of Power Sources, *31* (1990) 43 - 55

IMPROVED GELLED-ELECTROLYTE LEAD/ACID BATTERIES FOR DEEP-DISCHARGE APPLICATIONS

J. STREBE, B. REICHMAN, B. MAHATO and K. R. BULLOCK*

Corporate Applied Research, Johnson Controls, Inc., 5757 N. Green Bay Ave., Milwaukee, WI 53201 (U.S.A.)

Introduction

In many deep-discharge applications for lead/acid batteries, such as electric vehicle propulsion, load levelling, and solar energy storage, the need to add water to the battery can be prohibitively expensive. The electric vehicle tests run by the Department of Energy (DOE) in the U.S.A. have shown that the cost of adding water throughout the battery's life can be as high as the initial battery cost [1].

A low-maintenance lead/acid battery design with gelled electrolyte, developed by Johnson Controls, Inc. (JCI) for deep-discharge applications, is being tested both in the company's Load Management Test Facility and in the DOE electric vehicle program. This battery combines features from an advanced electric vehicle battery that was developed under the DOE aqueous mobile battery program** with Gel/Cell*** technology. The latter has been marketed for deep-discharge applications for more than 20 years.

Features of this design (which were taken from an electric vehicle battery to minimize weight and increase specific power and energy) include: an efficient radial grid design; a thin-walled poly(propylene) case; and low-resistance intercell welds. Characteristics that come from the Gel/Cell product line and give the battery its low-maintenance behaviour include: the addition of fumed silica to the sulphuric acid to produce a gel, a non-antimonial lead grid, a special separator design, and a one-way pressure relief valve on each cell to maintain a seal other than in the case of excessive pressure build-up. A proprietary lead/acid battery model was used to optimize the design for high specific energy and power.

An earlier report [2] described the performance of the GC6-1500B gelled-battery (Phase III). The purpose of this paper is to present performance data on the GC6-2000B (Phase IV) which is a modification of the

*Author to whom correspondence should be addressed.

**Subcontract No. A02000-234480 under DOE Contract No. DE-AC03-76CS51294.

***Registered trademark.

0378-7753/90/$3.50

earlier GC6-1500B gelled battery. The cycle life of the new modification showed a significant improvement under several discharge regimes.

Battery design

The first electric-vehicle battery developed under DOE Subcontract by the Battery Group of JCI (formerly Globe-Union, Inc.) in about 1976 was called the EV1000 [2]. An unusual feature of this design was that the plates were parallel to the length of the battery case rather than to its width. This approach was taken to increase the specific energy and power by reducing the total weight and increasing the efficiency of the grids. The EV1000 grid and case designs were later used to produce a series of low-maintenance, gelled-electrolyte batteries for electric vehicles. The latter were tested in fleet vehicles by the DOE.

The GC6-1500B was the third phase of the gelled-battery series. Each cell of the 6 V battery contained only 12 grids with a height of 19.9 cm and a width of 24.4 cm. Although this approach was effective in reducing weight, the non-standard grid size made the battery more costly to produce.

The Phase IV, GC6-2000B, was a further modification of the design, made to reduce the cost of the battery by using a standard grid size. This change also presented an opportunity to improve the cycle life by reducing the impact of the failure modes identified in the GC6-1500B [2]. The specific energy of the GC6-2000B was optimized, as it was in the GC6-1500B, by using the proprietary JCI lead/acid battery model to simulate performance of various design modifications. The GC6-2000B is now produced at rates comparable with automotive batteries for a wide variety of applications.

The most significant changes made in going from the GC6-1500B to the GC6-2000B have been as follows.

(i) The number of plates per cell was increased from 12 to 23 (11 positives, 12 negatives). These plates were sized smaller so that they could be placed parallel to the width rather than to the length of the case. The total geometric surface area of the positive plates was increased by only 1%.

(ii) Use of an outside negative plate increased the negative to positive ratio slightly, from 0.941 to 1.004. Gas-recombination characteristics were not changed by this modification.

(iii) The total grid weight increased by 118% for the positive electrodes and by 80% for the negative electrode. The positive grid thickness increased by 32% but the negative increased by only 1%. The contact area between the grid and the positive active material also increased because the plates were less over-pasted.

The overall effects of these changes were to decrease the specific energy by about 20% at a 75 A discharge rate, but to increase the deep-discharge cycle life by 168% and the total delivered energy by 148%. The drive cycle

life increased by 215%. The volumetric energy density decreased by only 4%. These effects will be discussed in more detail below.

Experimental

The data presented in this paper were obtained from extensive testing of both 6 V module units and 2 V single-cell units. Module testing was carried out on a programmable cycler and consisted of constant-current discharge and J227a/D drive cycling [3]. The J227a/D cycle includes: a high current, acceleration discharge; a moderate current, cruise discharge; a high current, regenerative braking charge; an open-circuit rest. The following comprise one sub-cycle:

(i) acceleration: −219 A for 25 s
(ii) cruise: −68 A for 50 s
(iii) regenerative braking: +101 A for 15 s
(iv) open-circuit rest: 0 A for 30 s

Under this cycling mode, the average current is −61 A. The 2 min cycling pattern is repeated until a 4.5 V per module cut-off limit is reached. An 8 h recharge is given immediately following each complete discharge.

End cells from full modules were used in single-cell testing after removal of the centre cell. These individual cells were tested under a constant-current, deep-discharge, cycling mode. Recharge of all modules and individual cells was carried out at constant current to a 2.35 V/cell limit, followed by current-taper charge. The 100% depth-of-discharge cycling was at 75 A discharge to a 1.70 V cut off, followed by charging of the GC6-2000B cell to a 35 A limit on cycles 1 - 350 and a 24 A limit on cycles 350 - 700, and charging of the GC6-1500B cell to a 24 A limit throughout the entire life span.

The single cells were all equipped with Hg/Hg_2SO_4 reference electrodes for half-cell measurements, temperature probes, and exit ports for determination of gas volume and composition. A real-time-based, computerized data acquisition system was used for continuous monitoring of the various cell parameters, including cell voltage and current, half-cell potentials, and temperature. The capacity and energy delivered were calculated from the various measurements. Each of the three cells of one module was equipped with tantalum probes and a reference electrode for cell voltage and half-cell measurements. A temperature probe inserted in the centre cell was used for temperature-correction of the charge voltage as well as for continuous monitoring of the temperature itself. All module and cell testing were carried out at ambient temperature, which varied between 23 and 28 °C.

At several points during the cycle test, the gassing characteristics of a cell were determined, including changes in the gassing rate during a charge/discharge cycle as well as the total gas volume and composition. The analysis of gas composition was carried out by a chromatographic method which has been previously described [4].

Results and discussion

Specifications for the GC6-2000B gelled-electrolyte battery are given in Table 1. In Fig. 1, complete cell voltage profiles of two individual end-cells, taken from the same module, are plotted against the amount of charge removed at three discharge currents. These data were taken from the first discharge after formation. As shown in the graph, the reproducibility of the single-cell data is quite good.

TABLE 1

Specifications for GC6-2000B battery

Dimensions (cm)	Length 32.64 ± 0.13 Width 18.29 ± 0.13 Height 21.59 ± 0.13 24.13 ± 0.30 (including terminals)
Weight (kg)	35
Nominal voltage (V)	6 (3 cells)
Internal resistance (mΩ)	~1.5
Capacity (A h @ 27 °C)	
@ 8.5 A (*C*/20 rate)	170
@ 15.0 A (*C*/10 rate)	150
@ 27.0 A (*C*/5 rate)	135
@ 102.0 A (*C*/1 rate)	102

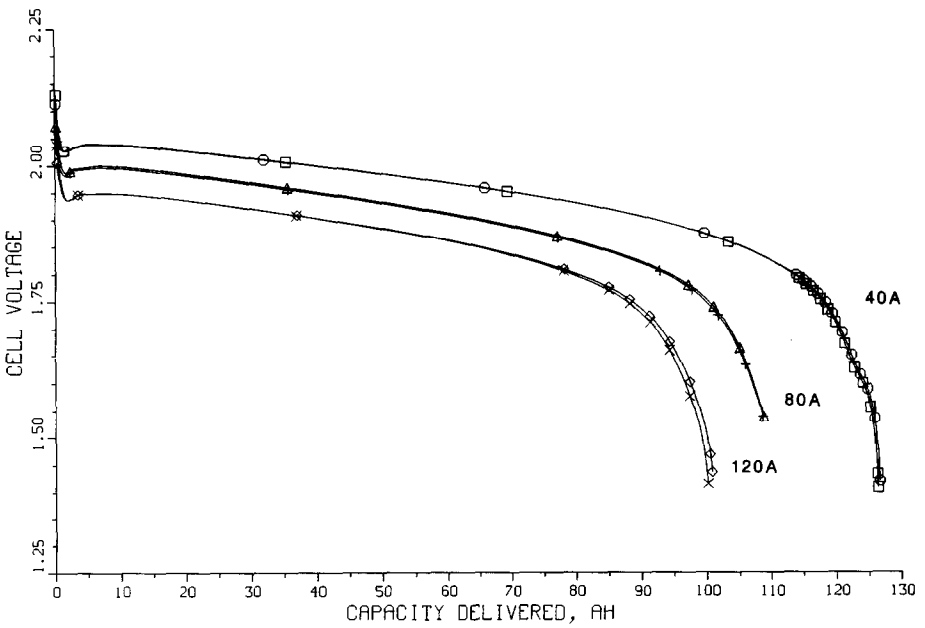

Fig. 1. Discharge curves at three discharge rates for two GC6-2000B cells.

JCI has developed a proprietary model that can be used to predict the discharge behaviour of lead/acid batteries [5 - 7]. The model can simulate a variety of service modes, including constant-current, constant-power, and constant-load discharges, as well as driving cycles with, or without, regenerative braking. The basic equations and assumptions used in the model have been described previously [5 - 7]. As reported earlier [2], the model was modified to accommodate the physical and electrochemical changes associated with the use of a gelled electrolyte in place of a liquid electrolyte and was used to design the GC6-2000B. The goals were to achieve both good specific energy and long, deep-discharge cycle life using components that would reduce production costs in a high-rate manufacturing process.

An empirical equation developed by Peukert [8], which is frequently used to predict the discharge capacity of a lead/acid battery design at any given discharge rate, is:

$$\log t = \log C - n \log i \tag{1}$$

where t is the discharge time in h, i is the discharge current in A, and n and C are constants that are characteristic of the battery design. A plot of $\log t$ *versus* $\log i$ thus gives a straight line that is called a Peukert plot. The Peukert plot predicted from the model for the GC6-2000B design is compared in Fig. 2 with the capacities taken from the discharge curves shown in Fig. 1. The closed circles show these initial capacities taken after formation. The square represents the highest capacity at about 120 cycles. As shown by the solid line, the model agrees closely with the highest capacity as well as with the slope of the Peukert plot. Linear regression analysis of the three initial

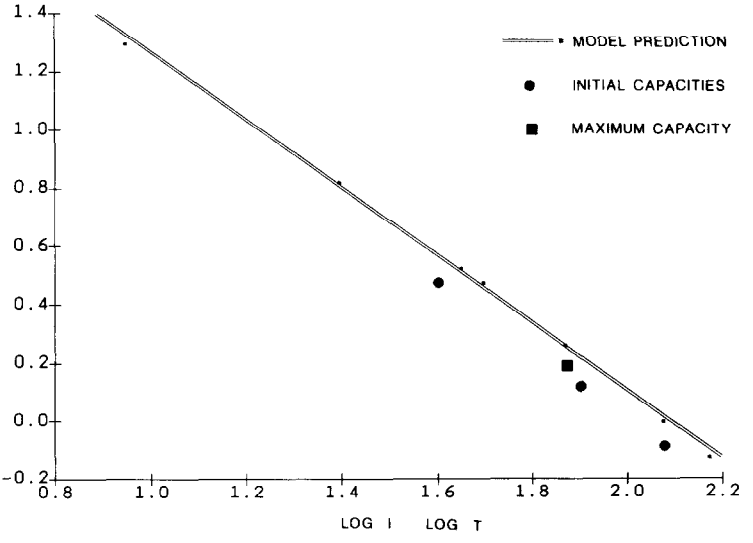

Fig. 2. Peukert plot for a GC6-2000B module. Points are experimental; line is predicted by model.

capacities gave n and C values of -1.181 and 2.366, respectively. The values of n and C determined from linear regression analysis of the model predictions in Fig. 2 are -1.163 and 2.432, respectively. The n and C values previously reported for the GC6-1500B were -1.238 and 2.553, respectively. The higher absolute value of n observed in the GC6-1500B is due to greater polarization at the higher discharge currents.

A 6 V battery was cycled under the J227a/D drive cycle regime described above. The voltage, temperature, and current traces during a typical drive cycle are given in Fig. 3. The various current steps during each sub-cycle, and the battery voltage in each step, are marked accordingly. The temperature trend (heavy line) shows, from left to right, a slow decrease to a minimum at the end of charge, followed by a more abrupt rise during discharge to a maximum of 33 °C at the end of discharge. Cooling of the free-standing battery was not necessary because this temperature trend remained consistent throughout cycling.

The peak performance of the GC6-2000B was 63 sub-cycles compared with 67 sub-cycles for the GC6-1500B. The approximate driving range for the J227a/D test is 0.93 miles/sub-cycle. This corresponds to a range of 59 miles for the GC6-2000B compared with 62 miles for the GC6-1500B. This decrease in range is small compared with the 215% improvement in cycle life shown by the GC6-2000B in this application.

A cycle summary plot displaying the number of sub-cycles accumulated per recharge cycle is given in Fig. 4. The graph shows that the capacity reached a maximum at close to 120 cycles and was maintained above the initial level through 420 cycles. For comparison, the cycle life previously reported [2] for the GC6-1500B is also shown in Fig. 4. The J227a/D cycle is

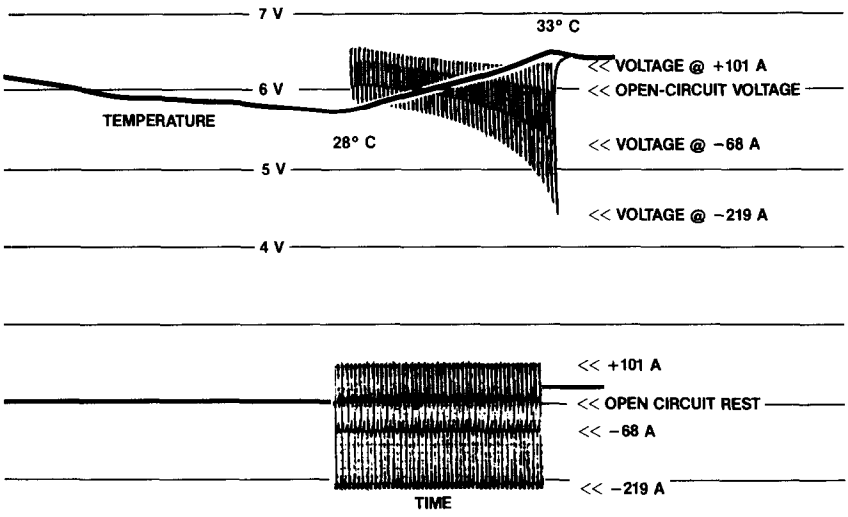

Fig. 3. Voltage and temperature profiles of GC6-2000B module during J227a/D drive cycle test.

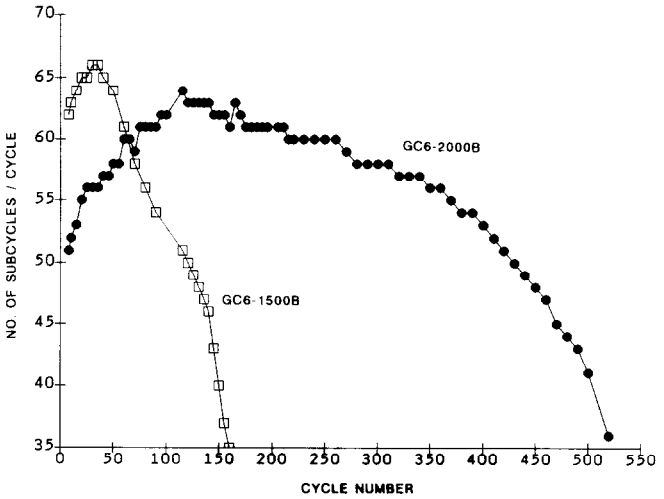

Fig. 4. Drive cycle testing of GC6-2000B and GC6-1500B module to 100% depth-of-discharge.

very severe due to the low voltage (1.5 V/cell) reached by the battery during the acceleration phase of the sub-cycle at the end of discharge. The changes made in the GC6-2000B to reduce the positive-plate polarization make it less sensitive to degradation due to this low cell voltage. The average end-of-discharge potential of the positive plate was about 110 mV higher in the GC6-2000B compared with the GC6-1500B.

Data on the cycle life of GC6-1500B and GC6-2000B test cells cycled under a constant-current discharge mode to 100% depth-of-discharge are given in Fig. 5. As in the drive cycle test, the GC6-2000B shows a slightly lower peak capacity but significantly better cycle life in the constant-current discharge cycle test. The GC6-2000B delivered 670 cycles to a 71.4 A h cut-off capacity, compared with 250 cycles for the GC6-1500B.

In flooded lead/acid batteries, acid stratification can lead to failure in deep-cycling applications unless acid circulation is incorporated into the cell design [9, 10] or the battery is severely overcharged to induce gassing. In gelled lead/acid batteries, however, acid stratification is not a significant cause of failure, and overcharge can be limited to 5% or less [11]. Limiting overcharge improves the cycling efficiency and minimizes grid corrosion and internal heating. Gassing is also reduced to a level where the oxygen cycle can function efficiently [12]. Neither the GC6-1500B nor the GC6-2000B failed because of either water loss or grid corrosion.

The half-cell potentials during discharge of the same GC6-2000B cell (*i.e.*, Fig. 5) are presented in Fig. 6 for cycles 1, 300, 500 and 700. The discharge current was 40 A, which corresponds to a $C/3$ rate based on the initial capacity. Both positive and negative electrodes show a capacity decrease with cycling. Since the positive electrode performance in the GC6-2000B is declining more slowly than in the GC6-1500B, the gradual

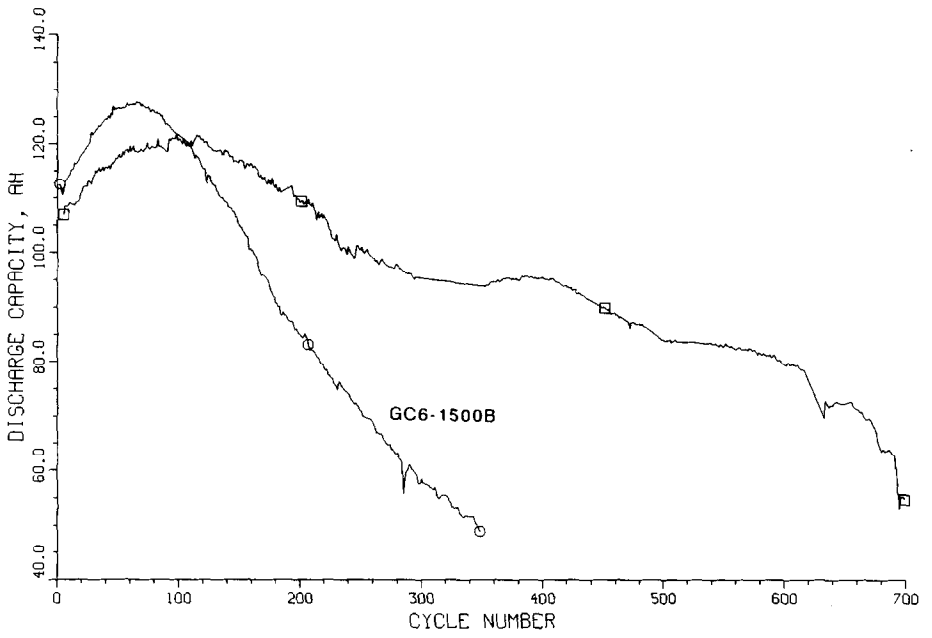

Fig. 5. Constant-current-discharge testing of GC6-2000B and GC6-1500B individual cells.

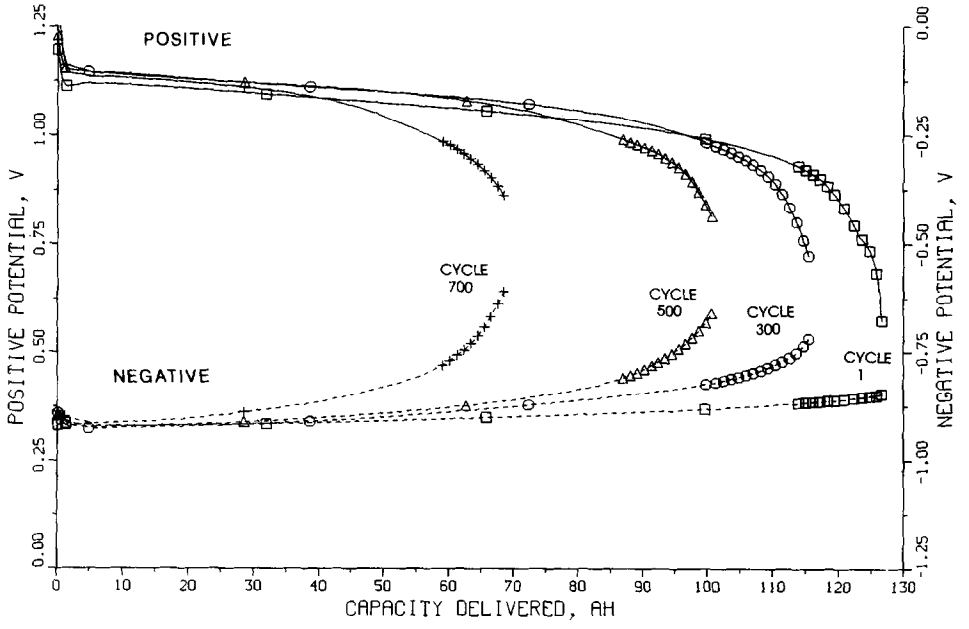

Fig. 6. Half-cell potentials of a GC6-2000B test cell as a function of cycle number.

TABLE 2

Capacity and specific energy of GC6-2000B and GC6-1500B batteries during 100% depth-of-discharge, constant-current cycling

	GC6-2000B	GC6-1500B
Maximum specific energy (W h kg^{-1} @ −75 A discharge current)	20	25
Maximum volumetric energy density (W h dm^{-3})	54.3	56.8
Cumulative capacity (A h)	65 000	26 500
Cumulative energy (kW h)	384	155
Battery volume (dm^3)	12.9	12.3
Battery weight (kg)	35	28
Cycle life (to 71.4 A h)	670	250
kW h kg^{-1} $cycle^{-1}$	0.0164	0.0221
Average voltage per cycle during discharge (V)	5.9	5.8

degradation of the negative plate can be observed. In the GC6-1500B, the more rapid capacity degradation was almost entirely due to the positive electrode.

Table 2 provides a summary of the total A h and W h capacities of 6 V modules based on the capacities accumulated during the cycle-life testing of the cells represented in Fig. 5. The total capacity in A h and energy in W h delivered by the GC6-2000B over its life is more than double that of the GC6-1500B. The GC6-2000B was designed to deliver 20% lower specific energy due to its increased grid weight, but this led to a 148% increase in the total energy delivered over the life of the battery.

It is interesting to note that the design changes in the GC6-2000B improved the drive cycle life even more than the constant-current-discharge cycle life. There are two obvious differences between these cycles. First, the average drive-cycle current of 61 A discharges a larger percentage of the active material than the 75 A for the constant-current-discharge cycle. Second, the drive cycle cut-off voltage is 1.5 V compared with 1.7 V for the constant-current discharge. The drive cycle polarizes the positive plate more due to the higher current during the acceleration phase of the sub-cycle.

Since the current densities were about the same and the differences in negative to positive active material ratios were not very great in the two modifications, the difference in average discharge currents cannot explain the greater improvement in drive cycle life shown for the GC6-2000B. However, the average positive plate potential at the end of discharge in the drive cycle was about 110 mV higher for the GC6-2000B. The thicker grid design and reduced overpasting in the GC6-2000B reduced the positive-plate polarization during the high-current acceleration phase of the sub-cycle and made the electrode less sensitive to degradation. This effect appears to be the major reason for the greater improvement in drive cycle life compared with the constant-current-discharge cycle life.

Figure 7 shows the capacity maintenance to a 1.53 V end-of-discharge voltage of another cell. This cell is normally being cycled at 80% depth-of-dis-

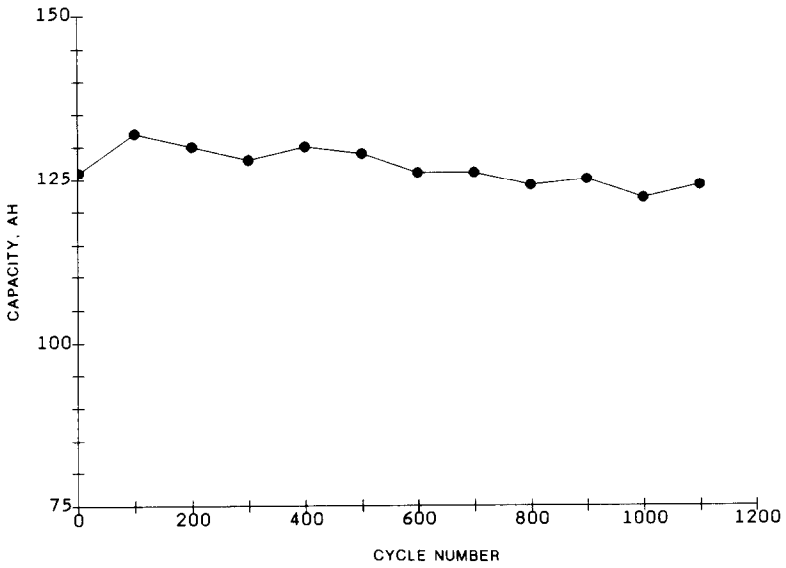

Fig. 7. 100% depth-of-discharge capacity *vs.* cycle number of GC6-2000B test cell being cycled at 80% depth-of-discharge.

charge, which is more representative of actual field usage in, for example, a load-levelling application. The capacity maintenance test, which is a constant-current discharge at −40 A to 100% depth-of-discharge to 1.53 V, is done periodically at 100-cycle intervals. The 80% depth-of-discharge cycling of this cell (based on initial capacity) consists of a 144 min discharge at −40 A followed by a 216 min charge at 35 A/2.35 V limit. Figure 8 shows the positive and negative half-cell potentials at the end of the discharge to 80% of initial capacity as a function of cycle number. The average end-of-discharge cell voltage is relatively constant. It is well known that cycling to 100% depth-of-discharge is a very severe test compared with shallower discharge cycling. In flooded batteries, for example, the cycle life at 80% depth-of-discharge is about twice that at 100% depth-of-discharge [9]. A similar difference in cycle life is evident in the gelled-electrolyte cell. This cell is still on test and has delivered nearly 1200 cycles thus far.

Recharge characteristics of the gelled-battery designs have been published previously [2, 11, 12]. In the recharge mode used in this study, the GC6-2000B battery reaches the voltage limit after at least 92 - 94% of the capacity is returned, and only about 5% overcharge is needed to maintain the capacity during deep cycling. Gassing rates and compositions on overcharge have been monitored during cycling by a method previously described. Gas-recombination efficiency in the GC6-2000B is very similar to that reported earlier for the GC6-1500B [2, 12].

The coulombic and energy efficiencies of the GC6-2000B cell shown in Fig. 5, which was cycled at 100% depth-of-discharge, are given in Fig. 9. From

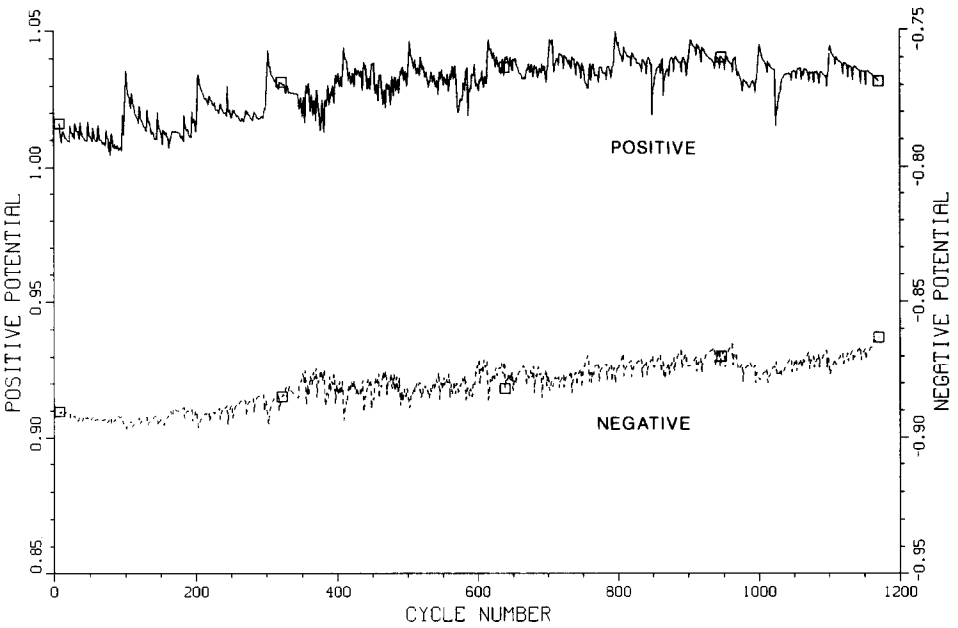

Fig. 8. End-of-discharge half-cell potentials of GC6-2000B test cell being cycled at 80% depth-of-discharge.

cycles 200 - 350, minor adjustments were made in charge current and cycle time to decrease the overcharge given per cycle. After cycle 350, the charge current was adjusted to 24 A. This resulted in a considerable improvement in charging efficiency. These efficiencies remained high throughout cycle life. This is similar to the previously reported data on the GC6-1500B [2].

Performance testing of the GC6-2000B battery demonstrates that gelled lead/acid batteries can have excellent cycle life in deep-discharge applications. As with flooded batteries, they can be designed with enough acid volume to achieve good reserve capacities; as with acid-immobilized lead/acid batteries, gelled lead/acid batteries operate on an oxygen cycle, reducing maintenance requirements. Because they recharge at a lower voltage limit than any other type of lead/acid battery [11] and require only minimal overcharge, gelled lead/acid batteries are also highly efficient and undergo minimal internal heating when properly recharged.

Conclusions

The GC6-2000B (Phase IV) modification shows significantly higher cycle life in both drive cycling and constant-current-discharge cycling tests

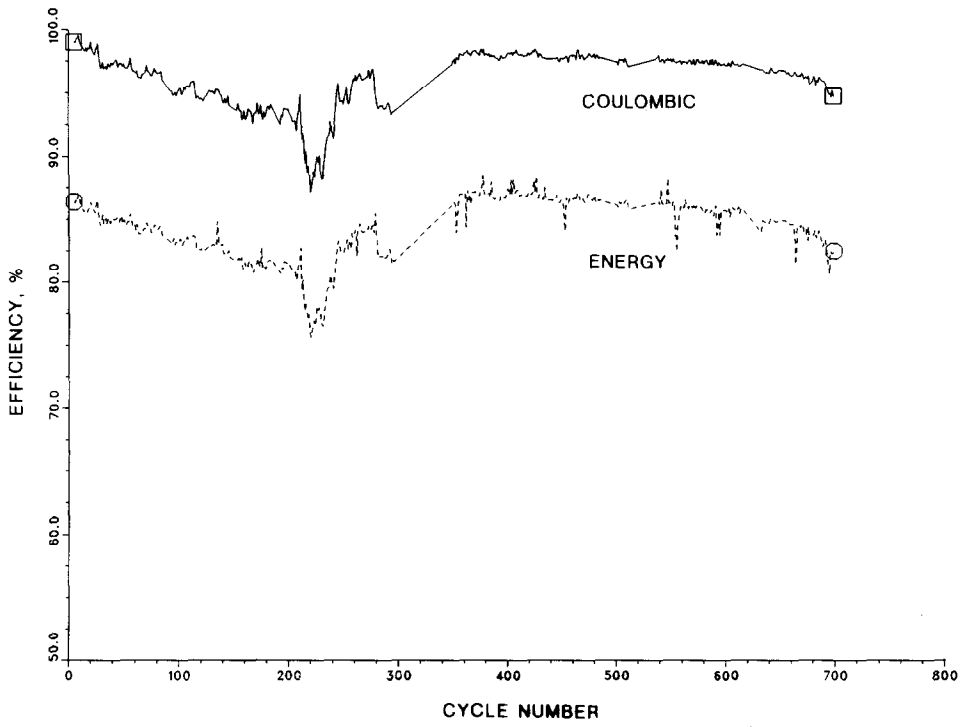

Fig. 9. Coulombic and energy efficiency during cycle testing of the GC6-2000B cell shown in Fig. 5.

than does the GC6-1500B (Phase III) modification reported previously [2]. The increase in life during the 100% depth-of-discharge cycling is about 168% (*i.e.*, from 250 to 670 cycles) and during J227a/D drive cycling it is about 215% (*i.e.*, from 165 to 520 cycles). Decreasing the polarization of the positive electrode at high currents appears to be the primary reason for the improvement. A cycle test at 80% depth-of-discharge, more representative of actual field usage, has yielded nearly 1200 cycles to date with little drop in capacity.

Use of the higher grid weights in the GC6-2000B has led to a 20% reduction in specific energy at a 75 A discharge rate, compared with the GC6-1500B. Because of better capacity maintenance, however, the total energy delivered over the cycle life is increased by 148%. The maximum volumetric energy density is only 4% lower than for the GC6-1500B.

The gas-recombination and overcharge characteristics of the GC6-2000B are similar to the GC6-1500B modification reported earlier [2, 12]. Both design modifications show good gas recombination, low maintenance, and high coulombic and energy efficiencies.

Acknowledgements

Development and testing of the GC6-1500B and GC6-2000B and development of the lead/acid model described in this paper were funded entirely by Johnson Controls, Inc.

The authors gratefully acknowledge the contributions of E. Laird, who determined the compositions of the gases. The GC6-1500B and GC6-2000B battery designs were developed and produced by the Specialty Battery Division of Johnson Controls, Inc. under the direction of T. Dougherty and M. Baxa. Helpful discussions with G. Brilmyer, M. Geibl, S. Gerner, D. Scarvaci and W. Tiedemann are gratefully acknowledged.

References

1 K. F. Barber, *Ext. Abstr. 6th Department of Energy Electrochemical Contractor's Review*, Washington, DC, 1984, p. 56.
2 B. K. Mahato and K. R. Bullock, in L. J. Pearce (ed.), *Power Sources 11*, International Power Sources Symposium Committee, Leatherhead, U.K., 1987, p. 149.
3 *Society of Automotive Engineers Handbook Part 2*, SAE, Inc., Warrendale, PA, 1981, p. 27.09.
4 K. R. Bullock and E. C. Laird, *J. Electrochem. Soc.*, *129* (1982) 1393.
5 W. Tiedemann and J. Newman, in S. Gross (ed.), *Proc. Symp. Battery Design and Optimization*, The Electrochem. Soc., *79-1* (1979) 23.
6 W. Tiedemann and J. Newman, Simulation of electric vehicle driving profiles based on mathematical models of the lead–acid battery system, presented at the *91st AIChE Meet.*, Detroit, MI, 1981.
7 W. Tiedemann and J. Newman, in K. R. Bullock and D. Pavlov (eds.), *Proc. Symp. on Advances in Lead–Acid Batteries*, The Electrochem. Soc., *84-14* (1984) 336.
8 W. Peukert, *Electr. Tech. Z.*, *18* (1897) 287.
9 K. R. Bullock, B. K. Mahato, G. H. Brilmyer and G. L. Wierschem, in K. R. Bullock and D. Pavlov (eds.), *Proc. Symp. on Advances in Lead–Acid Batteries*, The Electrochem. Soc., *84-14* (1984) 451.
10 G. L. Wierschem and W. H. Tiedemann, *Ext. Abstr.*, The Electrochem. Soc., *80-2* (1980) 278.
11 B. L. McKinney, B. K. Mahato and K. R. Bullock, in K. R. Bullock and D. Pavlov (eds.), *Proc. Symp. on Advances in Lead–Acid Batteries*, The Electrochem. Soc., *84-14* (1984) 426.
12 J. S. Symanski, B. K. Mahato and K. R. Bullock, *J. Electrochem. Soc.*, *135* (1988) 548.